UNIVERSITÄT AUGSBURG
Universitätsbibliothek

OPEN ACCESS
OPUS AUGSBURG

Driving the mid-latitude ionosphere from below: a statistical study using LOFAR

Alan G. Wood, Maaijke Mevius, Richard A. Fallows, Juliana Jaen, Gareth D. Dorrian, Ben Boyde, Katarzyna Beser, Pietro Zucca, Mattia Mancini, Corwin J. Wright, Neil P. Hindley, Carsten Schmidt, Jaroslav Urbář, Michael Bittner, Mario Bisi, Leszek Blaszkiewicz, Tobia D. Carozzi, Claudio Cesaroni, Agata Chuchra, Jaroslav Chum, Helena Ciechowska, Bartosz Dabrowski, Sean Elvidge, Pawel Flisek, Biagio Forte, Martin Füllekrug, Rebecca Ghidoni, Patrick Hannawald, Edmund Henley, David Jackson, Rosie Johnson, Kacper Kotulak, Petra Koucká Knížová, Mark Kuiack, Andrzej Krankowski, Lisa Küchelbacher, Šimon Mackovjak, Barbara Matyjasiak, Mariusz Pożoga, Thi Phung, Dorota Przepiórka, Yuriy G. Rapoport, Hanna Rothkaehl, Luca Spogli, Jānis Šteinbergs, Claudia Stolle, Lukasz Tomasik, Vladimír Truhlík, Ralph Wijers, Sabine Wüst

Angaben zur Veröffentlichung / Publication details:

Wood, Alan G., Maaijke Mevius, Richard A. Fallows, Juliana Jaen, Gareth D. Dorrian, Ben Boyde, Katarzyna Beser, et al. 2026. "Driving the mid-latitude ionosphere from below: a statistical study using LOFAR." *Journal of Space Weather and Space Climate* 16: 30. https://doi.org/10.1051/swsc/2026023.

Nutzungsbedingungen / Terms of use: **CC BY 4.0**

Dieses Dokument wird unter folgenden Bedingungen zur Verfügung gestellt: / This document is made available under these conditions:
CC-BY 4.0: Creative Commons: Namensnennung
Weitere Informationen finden Sie unter: / For more information see:
https://creativecommons.org/licenses/by/4.0/deed.de

J. Space Weather Space Clim. 2026, **16**, 30
© A. Wood et al., Published by EDP Sciences 2026
https://doi.org/10.1051/swsc/2026023

JSWSC
Available online at:
www.swsc-journal.org

RESEARCH ARTICLE OPEN ACCESS

Driving the mid-latitude ionosphere from below: A statistical study using LOFAR

Alan G. Wood[1,2,*], Maaijke Mevius[3,4], Richard A. Fallows[5], Juliana Jaen[6], Gareth D. Dorrian[1], Ben Boyde[7], Katarzyna Beser[8], Pietro Zucca[3], Mattia Mancini[3], Corwin J. Wright[6], Neil P. Hindley[6], Carsten Schmidt[9], Jaroslav Urbář[10], Michael Bittner[9,11], Mario Bisi[5], Leszek Blaszkiewicz[12], Tobia D. Carozzi[13], Claudio Cesaroni[14], Agata Chuchra[15], Jaroslav Chum[10], Helena Ciechowska[15], Bartosz Dabrowski[12], Sean Elvidge[1], Pawel Flisek[12], Biagio Forte[7], Martin Füllekrug[6], Rebecca Ghidoni[14], Patrick Hannawald[9], Edmund Henley[2], David Jackson[2], Rosie Johnson[16], Kacper Kotulak[12], Petra Koucká Knížová[10], Mark Kuiack[17], Andrzej Krankowski[12], Lisa Küchelbacher[9], Šimon Mackovjak[18], Barbara Matyjasiak[15], Mariusz Pożoga[15], Thi Phung[15], Dorota Przepiórka[15], Yuriy G. Rapoport[12], Hanna Rothkaehl[15], Luca Spogli[14], Jānis Šteinbergs[19,20], Claudia Stolle[21], Lukasz Tomasik[15], Vladimír Truhlík[10], Ralph Wijers[17], and Sabine Wüst[9]

[1] Space Environment and Radio Engineering (SERENE) group, University of Birmingham, Edgbaston, Birmingham, B15 2TT, UK
[2] Met Office, FitzRoy Road, Exeter, EX1 3PB, UK
[3] ASTRON – The Netherlands Institute of Radio Astronomy, Oude Hoogeveensedijk 4, 7991 PD Dwingeloo, The Netherlands
[4] Kapteyn Astronomical Institute, University of Groningen, P.O. Box 800, 9700 AV Groningen, The Netherlands
[5] RAL Space, United Kingdom Research and Innovation – Science & Technology Facilities Council – Rutherford Appleton Laboratory, Harwell Campus, Oxfordshire, OX11 0QX, UK
[6] Center for Climate, Adaptation and Environment Research, University of Bath, BA2 7AY, Bath, UK
[7] Department of Electronic and Electrical Engineering, University of Bath, BA2 7AY, Bath, UK
[8] New Jersey Institute of Technology, 323 Dr Martin Luther King Jr Blvd, Newark, NJ 07102, USA
[9] German Remote Sensing Data Center (DFD), German Aerospace Center (DLR), 82234 Oberpfaffenhofen, Germany
[10] Institute of Atmospheric Physics of the Czech Academy of Sciences, Boční II, Prague 4, Czech Republic
[11] Institute of Physics, University of Augsburg (UNA), 86159 Augsburg, Germany
[12] Space Radio-Diagnostics Research Center, University of Warmia and Mazury in Olsztyn, Michala Oczapowskiego, 10-719 Olsztyn, Poland
[13] Department of Space, Earth and Environment, Onsala Space Observatory, Chalmers University of Technology, 43992 Onsala, Sweden
[14] Istituto Nazionale di Geofisica e Vulcanologia, Via di Vigna Murata 605, 00143, Roma, Italy
[15] Centrum Badań Kosmicznych Polskiej Akademii Nauk, Bartycka 18 A, 00-716 Warsaw, Poland
[16] Department of Physics, Aberystwyth University, Aberystwyth, SY23 3BZ, UK
[17] Anton Pannekoek Institute of Astronomy, University of Amsterdam, Science Park 904, P.O. Box 94249, NL-1090 GE, The Netherlands
[18] Department of Space Physics, Institute of Experimental Physics, Slovak Academy of Sciences, 040 01 Košice, Slovakia
[19] Riga Technical University, 6A Kipsalas Street, Rīga, LV-1048, Latvia
[20] Ventspils International Radio Astronomy Center, Engineering Research Institute, Ventspils University of Applied Sciences, Ventspils, LV-3601, Latvia
[21] Leibniz Institute for Atmospheric Physics, University of Rostock, 18225 Kühlungsborn, Germany

Received 18 December 2025 / Accepted 29 May 2026

Abstract – The Low Frequency Array (LOFAR) is one of the most advanced radio telescopes in the world. When radio waves from a distant astronomical source traverse the ionosphere, structures in this plasma affect the signal. Results are presented from a statistical study using 2,810 hours of observations of Cassiopeia A from a LOFAR station located in the Netherlands (station CS032, located at 52.9° N; 6.9° E) between 28th June 2014 and 27th November 2016. Ionospheric structures were identified in 469 (∼17 %) of these observations. A comparison with proxies for geomagnetic activity (the K_p index) and

*Corresponding author: alan.wood@metoffice.gov.uk

This is an Open Access article distributed under the terms of the Creative Commons Attribution License (https://creativecommons.org/licenses/by/4.0), which permits unrestricted use, distribution, and reproduction in any medium, provided the original work is properly cited.

solar activity (the F10.7 cm solar radio flux) showed that geomagnetic or solar effects were not the primary driver of these ionospheric structures. Ionospheric structures were more common in summer and between ∼21 LT and 02 LT. These patterns in season and local time showed similarities to the occurrence of lightning strikes. When ionospheric structures were present, the mean number of lightning strikes in a spatial region close to the LOFAR observations (51.9° – 56.5° N; 3.9° – 9.9° E) two hours prior to the LOFAR observations was (70 ± 25) per hour. This was substantially larger than the mean value of (19 ± 5) per hour when the ionospheric structures were absent. This suggests that quasi-upward propagating Atmospheric Gravity Waves (AGWs) launched by thunderstorm activity could be one of the sources of the ionospheric structures. Collectively, these observations show that LOFAR can be used to infer ionospheric signatures of vertical coupling processes in the mid-latitude atmosphere. Such observations have the potential to be used to develop or validate existing Global Circulation Models (GCMs) or new models of vertical coupling within the terrestrial atmosphere.

Keywords: Ionospheric Physics / Space weather / Neutral Atmosphere / Thunderstorms / Radio Astronomy

1 Introduction

The Low Frequency Array (LOFAR; van Haarlem et al., 2013) is one of the most advanced radio telescopes in the world. When radio waves from a distant astronomical source traverse the ionosphere, structures in this plasma affect the signal. These observations can be used to infer the properties of the ionosphere. This is not a new idea; prior to the space age, the only practical way to study the topside ionosphere was to observe the effect of the terrestrial plasma on trans-ionospheric radio signals of extraterrestrial origin (Payne-Scott & McCready, 1948) or on signals of terrestrial origin which were subsequently reflected by the Moon (Kerr et al., 1949). The plasma structures causing the variations could be located anywhere on the ray path, and so, when an extraterrestrial radio source was used, there was uncertainty about the location of these structures. Little & Lovell (1950) observed the radio sources Cygnus A (RA: 299.87°; Dec: 40.73°) and Cassiopeia A (RA: 350.85°; Dec: 58.82°) with radio telescopes located at Cambridge (52.2° N; 0.1° E) and Jodrell Bank (53.2° N; 2.3° W). On the basis of the scale size of the structures observed, it was suggested that the plasma structures were located in the ionosphere as opposed to the interstellar medium. Dagg (1957) observed Cassiopeia A for a year from Inverness (∼57° N; ∼4° W) at a frequency of 79 MHz. Ionospheric variability was greatest in the evening and in the months of April, May, and June. No one-to-one correlation was found with magnetic activity, but there was some indication of an underlying trend.

The new generation of radio telescopes, of which the LOFAR is one, enables the terrestrial effects on trans-ionospheric radio waves to be observed with an unprecedented level of detail. The high temporal resolution available (∼10 ms), the range of frequencies observed (10–90 MHz and 110–250 MHz), the large number of receiving stations (currently 52 across Europe), and the availability of a wide variety of complementary instruments enable such observations.

The Kilpisjärvi Atmospheric Imaging Receiver Array (KAIRA) in northern Finland (69.7° N; 20.8° E) uses LOFAR antennas and digital signal-processing hardware, although there are some differences in how these antennas are arranged and operated (McKay-Bukowski et al., 2014). Fallows et al. (2014) demonstrated that this instrumentation could observe ionospheric effects through variations in the intensity of the received signal when observing Cygnus A at frequencies between 30 and 250 MHz. The capability of LOFAR to observe such effects in the mid-latitude region over Europe was demonstrated by Fallows et al. (2016). Subsequent case studies using LOFAR have shown two Travelling Ionospheric Disturbances (TIDs) simultaneously (Fallows et al., 2020), the presence of a Small Scale TID (SSTID; Boyde et al., 2022), substructure within a Medium Scale Travelling Ionospheric Disturbance (MSTID; Dorrian et al., 2023), substructure within a sporadic-E layer (Wood et al., 2024), and symmetric quasi-periodic scintillations (Trigg et al., 2024). The small-scale sizes of many of these features (kilometres to tens of kilometres) imply a local source, either due to instability processes in the mid-latitude ionosphere or due to drivers from below. LOFAR can also observe ionospheric effects associated with geomagnetic storms. Ghidoni et al. (2025a) showed that, during a minor geomagnetic storm that occurred in January 2022, LOFAR scintillation was driven by increased direct particle precipitation in the auroral oval, steepening of the ionospheric trough's equatorward edge, and the equatorward propagation of small-scale, high-velocity (≥ 800 m/s) wave structures. Ghidoni et al. (2025b) reported that, during the May 2024 geomagnetic superstorm, there was significant signal fading associated with the equatorward expansion of the auroral oval during the main phase of the storm, and there was intense scintillation during the recovery phase. This intense scintillation located at an unusually high altitude (up to 1500 km) was linked to fast-moving ionospheric irregularities, with drift velocities reaching ∼800 m s^{-1}.

It is assumed that the radio waves from an extraterrestrial radio source are in phase at the top of the atmosphere, although the phase itself is unknown. As these radio waves pass through the ionosphere, they experience phase changes in proportion to the Total Electron Content (TEC, the integral of electron density along the line of sight). Mevius et al. (2016) used LOFAR to infer the difference in TEC (dTEC) on numerous pairs of ray paths with different separations in order to determine the amount of structuring in the mid-latitude ionosphere on different spatial scales. TIDs appear in dTEC measurements as waves, and Beser et al. (2022) identified variations in dominant wave direction over the course of several hours. A methodology has been developed to determine the propagation direction, speed, and amplitude of waves observed in the ionosphere (Boyde et al., 2024), and a climatology has been created using this method. The waves observed primarily propagate in the opposite direction to the prevailing wind, which strongly suggests

that the structures observed are the ionospheric manifestation of upward propagating Atmospheric Gravity Waves (AGW; Boyde et al., 2025). This implies that the majority of the plasma structures observed in this climatology are driven by variability lower in the terrestrial atmosphere. The results of Boyde et al. (2025) agree with the statistical results obtained by independent measurements using a multi-point continuous Doppler sounding (Chum et al., 2021).

The ionosphere is structured on a wide range of spatial and temporal scales. Variations on spatial scales from a few meters to thousands of kilometres, and temporal scales ranging from seconds to more than a solar cycle have been widely reported in the published literature. The underlying physical processes have been summarised by Hargreaves (1992). Of particular relevance to the present study are TIDs resulting from AGWs. AGWs typically originate in the lower atmosphere and can be launched by orography, thunderstorms, fronts, baroclinic instabilities in the troposphere, volcanic eruptions, and the excitation of waves associated with the polar vortex (Fritts & Alexander, 2003). These waves propagate upwards, growing in amplitude with increasing altitude (Hines, 1960). They perturb both the atmospheric temperature and wind. When the AGWs cause the temperature variations as a function of altitude to exceed the adiabatic lapse rate, then the atmosphere becomes unstable and the wave breaks. The deposition of energy and momentum into the atmosphere can rotate the wind vector, significantly altering the atmospheric circulation (Holton, 1992). This results in global effects, including changes in atmospheric density, the atmospheric composition, and elevated temperatures over the winter pole (Holton & Hakim, 2013). AGWs have an ionospheric manifestation; the perturbations that they introduce are observed as TIDs. AGWs are also commonly referred to as Gravity Waves (GWs). However, to avoid confusion with Gravitational Waves (also referred to as GWs within the astronomical community), the term AGW will be used throughout the present paper.

AGWs associated with thunderstorm activity and those with an orographic source are of particular relevance to the present study. A horizontal wind over mountainous terrain launches AGWs not just at this location, but also further downstream as a given volume of air oscillates with damped simple harmonic motion. AGWs have a component of their phase velocity that propagates in the opposite direction to the horizontal background wind. If the velocity of the wind varies with altitude, then the AGW is refracted. If there is a reversal of the wind velocity, then the wave cannot propagate unless its phase velocity is higher than the wind velocity and breaking occurs. It is possible for this process to perturb the atmosphere sufficiently to launch secondary AGWs (Vadas et al., 2018). The propagation of AGWs is strongly affected by the background conditions, which vary over time (Fritts et al., 2006). The mesospheric and lower thermospheric winds, planetary waves, and tides change with local time and season. These phenomena, and the interactions between them, all play roles in the modulation of the wave propagation conditions. This, in turn, influences which of these AGWs are capable of causing ionospheric effects.

In addition, planetary waves driven by the Coriolis force and with wavelengths of hundreds to thousands of kilometres are important in mid-latitude circulation patterns on time scales between two days and approximately 20 days (e.g., causing the occurrence sequence of low- and high-pressure systems in the troposphere). While planetary waves themselves are usually not able to propagate into the ionosphere, they affect the upper atmosphere indirectly by modifying both sources and propagation conditions of other waves, especially AGWs (Manson et al., 2003).

The purpose of this paper is to present a statistical study of observations of ionospheric structures observed by LOFAR and the possible drivers of these structures. The paper is arranged as follows. Section 2 details the instrumentation and dataset. Section 3 discusses the data processing. The results are presented in Section 4, followed by a discussion in Section 5. Conclusions are drawn in Section 6.

2 Instrumentation and dataset

The LOFAR radio telescope (van Haarlem et al., 2013) operates at HF/VHF frequencies from 10 − 250 MHz, with a gap between 90–110 MHz for the FM band, which is used by commercial and publicly-owned broadcasters. It comprises Low Band Antennas (LBA), which can observe in the frequency range 10 − 90 MHz, while the High Band Antennas (HBA) can observe in the frequency range 110 − 250 MHz. At the time of writing, LOFAR has 52 stations, 38 of which are located in the Netherlands. The radio astronomy observations conducted using LOFAR include both beam-formed observations in the time domain and radio interferometry. The present study uses observations of Cassiopeia A made using the LBA at a frequency of 44.3 MHz.

A dedicated ionospheric scintillation experiment was first run using LOFAR in 2013, with initial results published in Fallows et al. (2020). Since 2014, this has been run as a "filler time" experiment, observing during a selection of times when LOFAR was not being used for radio astronomy observations. A series of case studies have been published (Fallows et al., 2016; Boyde et al., 2022; Dorrian et al., 2023; Wood et al., 2024; Trigg et al., 2024; Ghidoni et al., 2025a, 2025b); however, the file sizes of the observations (approximately 40 GB per hour) and the process needed to extract data from the LOFAR Long Term Archive (LTA) have, to date, precluded a statistical study using these data.

A new pipeline has recently been developed to process and downsample observations from the LOFAR ionospheric scintillation experiment in order to create a smaller data product that is more readily available to the research community. In this pipeline, points contaminated by Radio Frequency Interference (RFI) were identified by applying a median filter to the data using a window of 976.5 kHz × 4.2 s, which flattened out the scintillation pattern, and then applied a threshold of five sigma above the average value to identify the RFI. Data points above this threshold were replaced by an interpolation from nearby data, using the Python Astropy (Astropy Collaboration et al., 2013; Price-Whelan et al., 2018) library routine, "interpolate_replace_nans"; this entire method was outlined in Fallows et al. (2020). The observations were then broken into intervals of a maximum of one hour, with break points at the start of each hour. They were then downsampled to a temporal resolution of 1 s, which reduced both the data volume and the noise. Prior to

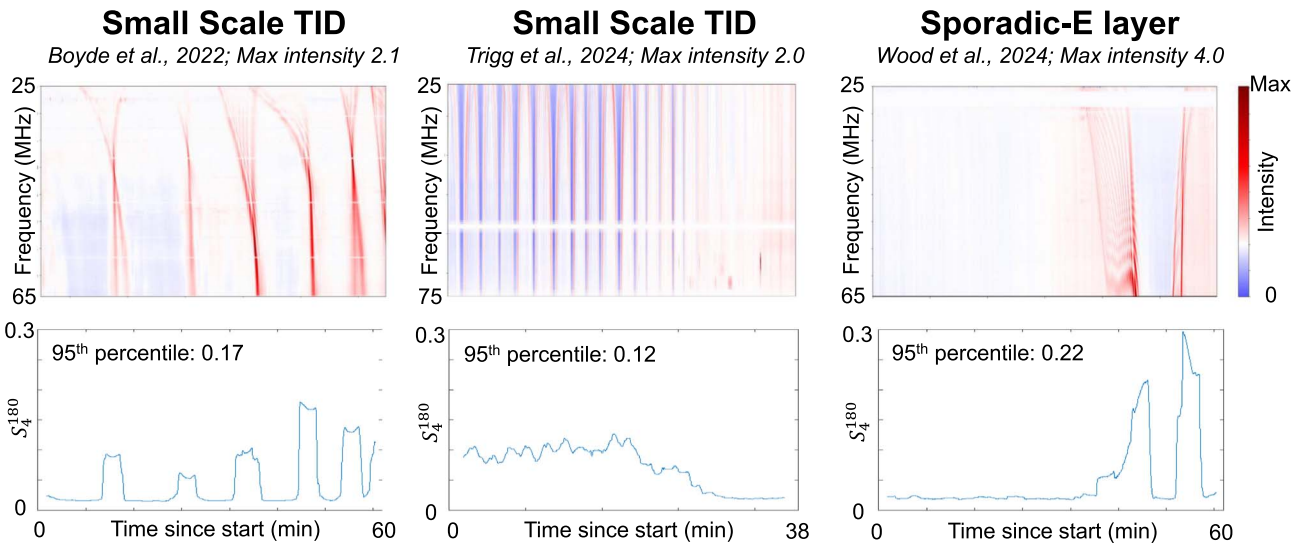

Figure 1. The dynamic spectrum (top row) showing the relative signal intensity as a function of time and of frequency for observations of astronomical radio sources of SSTIDs (Boyde et al., 2022; Trigg et al., 2024) and variations within a sporadic-E layer (Wood et al., 2024). These data have been reprocessed to match the methodology used in the present study. The intensity scales differ between the panels to improve the clarity of this figure. In each case, the minimum value of the intensity scale is zero, and the maximum value is given in the panel heading. The left and right panels both have a duration of one hour; however, the middle panel has a shorter duration of 38 min, as this was the length of the observation. Horizontal white regions correspond to frequency channels removed due to significant radio frequency interference. The lower panels show S_4^{180} as a function of time at a frequency of 44.3 MHz, together with the 95th percentile of this time series.

this down-sampling, the ionospheric scintillation index S_4 (Briggs & Parkin, 1963) was calculated across intervals of 60 seconds and 180 seconds at each frequency. These are referred to as S_4^{60} and S_4^{180}, respectively. At the time of writing, this pipeline has been applied to observations from the ionospheric scintillation experiment conducted between 28th June 2014 and 27th November 2016 (inclusive).

To create the dataset used within the present paper, all observations that had been processed via the pipeline were considered. Data were selected if the observation contained at least 54 min of data within the stated hour. Data were initially used at one frequency (44.3 MHz) and at one station (CS032; 52.9° N; 6.9° E). This frequency was chosen as it was in the centre of the range of frequencies observed with the LBA in this experiment. CS032 was chosen as this station was later used for extended (multi-year) solar and ionospheric observations as part of the Incremental Development of LOFAR Space Weather (IDOLS) programme. Using the same station in the present study will better enable comparisons with IDOLS as these data become more readily available to the research community.

The measure of ionospheric variability chosen was S_4^{180}, as Wood et al. (2024) showed that this time interval captured the ionospheric variability better than S_4^{60}, because the timescale of the variations in the relative signal intensity, which were of interest, exceeded 60 s. The 95th percentile of S_4^{180} was taken during each observation[1] and used as a measure of the variability of the ionosphere in that hour (Supplementary Material 1). To enable the subsequent statistical analysis, a threshold needed to be chosen for the 95th percentile of S_4^{180} which, if exceeded, would count as an event. To determine this limit, S_4^{180} was calculated for the relative signal intensities used in a selection of previously published studies (Boyde et al., 2022; Trigg et al., 2024; Wood et al., 2024), which are reproduced in Figure 1. These studies were selected based on data availability. The 95th percentile of S_4^{180} at 44.3 MHz was found to be 0.17, 0.12, and 0.22, respectively, for these studies. On this basis, a threshold of $S_4^{180} > 0.1$ was selected. It must be emphasised that this threshold, and the choice of the 95th percentile, are intended to be sensible starting points for this initial statistical study based on the information available to date. These choices should be revisited and will likely need to be revised as additional studies are conducted. Rapid variations in the intensity of the received signal resulting from the interference of the refracted radio waves are known as spectral caustics (Clegg et al., 1998). Koval et al. (2017) used the Nançay Decametric Array (NDA) to observe the Sun at frequencies within the range of 10–80 MHz. Variations in the intensity of the received signal due to the effect of the ionosphere were observed and described as spectral caustics. At least a subset of the observations used within the present study fulfil the definition of spectral caustics. The example shown in the top right-hand panel of Figure 1 has previously been described in this manner (Wood et al., 2024). However, without manually inspecting every observation processed in the new LOFAR data processing pipeline, it is not known whether there is a one-to-one correspondence between spectral caustics and the variations reported in the present study. Therefore, the term spectral caustics is not used further within the present paper.

In order to proceed with the statistical analysis, proxies for geophysical activity and solar activity were selected and associated with the dataset. The proxies chosen were the K_p index (Mayaud, 1980) and the F10.7 cm solar radio flux (Tapping, 2013), respectively. Lightning strike data were obtained from the Arrival Time Difference NETwork (ATDNet), which uses

[1]As S_4^{180} was calculated after the observations were broken into segments of not more than one hour, S_4^{180} was not calculated for timestamps within the first or last 90 seconds of each observation.

a series of radio receivers across Western Europe to detect the broadband radio emission from lightning (Lee, 1989). The number of lightning strikes per hour, and up to six hours previously, was associated with the dataset.

Proxies for planetary wave activity and gravity wave activity were also associated with the dataset. These wave activity proxies are based on temperature variability as determined from OH airglow observations in the upper mesosphere at a range of altitudes spanning approximately 7 km and centred on 86–87 km. These proxies are therefore sensitive to waves which occur at these altitudes. Several such observations are performed with identical ground-based infrared spectrometers at different sites across Europe (Schmidt et al., 2013), all of which are part of the Network for the Detection of Mesospheric Change (NDMC). At the time of writing, for the time period covered by this study, the wave activity proxies derived from these observations are available for a few sites only, with the Environmental Research Station "Schneefernerhaus" (UFS), Germany (47.04° N; 10.98° E) being closest to LOFAR. UFS is the reference site of the NDMC network and stands out due to its superior data quality (Schmidt et al., 2023).

The proxy for planetary wave activity is based on nocturnal mean temperatures and calculated following the methodology outlined by Höppner & Bittner (2007). Essentially, the total statistically significant spectral intensity, determined by means of a wavelet analysis in the period range relevant for planetary waves (3–20 days), is summed and provided on a monthly basis. The gravity wave activity is based on calculating the actual potential energy density (GWPED) of the waves by retrieving estimates of the wave periods and power from the high-temporal resolution (one minute) observations. Details of calculating the GWPED are given in Wüst et al. (2016).

3 Data processing

Variations in S_4^{180}, which were interpreted as plasma structures, were present in 469 of the 2,810 hours (~17%) of observations in the dataset, and these 469 hours are hereafter referred to as "events". The plasma structures associated with these events can be located anywhere on the path traversed by the radio wave from the astronomical source to the receiving station. However, in practice, ionospheric structures can be identified based on their scale. Little & Lovell (1950) observed the fluctuations in the intensity of the signal received from an astronomical radio source and found that these variations were highly correlated on a baseline of 100 m, had a correlation of between 0.5 and 0.95 on a baseline of 3.9 km, and were uncorrelated on a baseline of some 200 km. On the basis of the scale size, they concluded that the variations observed were due to plasma structures in the ionosphere. Some ionospheric structures are asymmetric, and variations in signal intensity are more highly correlated in one direction than another (e.g., Wood et al., 2024). To determine whether the plasma structures observed in the present study were located in the ionosphere, additional checks were undertaken. Correlations between the relative signal intensity at a frequency of 44.3 MHz at LOFAR stations CS032 and RS210 (52.3° N; 6.9° E) were determined for the hours in which events occurred. This analysis was repeated for LOFAR station CS032 and RS310 (52.7° N; 6.1° E). Stations RS210 and RS310 were chosen as they were stations in the Netherlands with the longest possible baselines to CS032 in approximately orthogonal directions (approximately 65 km in the north–south direction and approximately 50 km in the east–west direction). If the correlation between CS032 and both remote stations exceeded 0.9, then this event was flagged as having a scale size that could place it outside of the ionosphere. Data from stations RS210 and RS310 were not always available, so only 2,558 h of observations were tested in this manner. A total of 12 events were identified as having a scale size that could place them outside of the ionosphere. The majority of the plasma structures observed had scale sizes that placed them inside the ionosphere.

4 Results

K_p and $F_{10.7}$ are proxies for geomagnetic and solar activity, respectively. Figure 2 shows the number of hours of observations in the dataset for three different ranges of the K_p index, together with the proportion of hours in the dataset containing events in these ranges. The ranges of the K_p index chosen were $K_p < 2$, $2 \geq K_p \geq 4$ and $K_p > 4$. While it is appreciated that $K_p = 4$ does not correspond to a particularly extreme event, this level was chosen to maintain a reasonable number of hours in the dataset for this upper category. The proportion of hours which contain events increased with increasing K_p, but a greater number of events (179) occurred at low K_p ($K_p < 2$) than at high K_p (41 events at $K_p > 4$). Also shown in Figure 2 is a similar analysis for three different levels of the F10.7 cm solar radio flux. The ranges selected were $F_{10.7} < 120$ sfu, 120 sfu $\geq F_{10.7} \geq 150$ sfu and $F_{10.7} > 150$ sfu. The proportion of hours that contain events increased with increasing $F_{10.7}$, but a greater number of events occurred for low values of this index ($F_{10.7} < 120$ sfu). The Hinode Flare Catalogue (Watanabe et al., 2012) showed that M-class flares occurred during 10 h within the dataset when the Sun was above the horizon; however, no events were observed in any of these hours. These hours were 9th November 2014 (11–12 UT), 15th March 2015 (9–10 UT), 20th June 2015 (6–7 UT & 7–8 UT), 27th September 2015 (10–11 UT), 28th December 2015 (11–12 UT, 12–13 UT, 13–14 UT & 14–15 UT) and 13th February 2015 (15–16 UT). No X-class flares occurred in any hour in the dataset when the Sun was above the horizon. A possible reason why M-class flares did not result in ionospheric structures observed by LOFAR is that the flares may have raised the ionospheric density uniformly. Wood et al. (2024) observed the effects of a sporadic-E layer on radio waves using LOFAR and showed that the variations that occurred were a result of variations ***within*** a sporadic-E layer, rather than being associated with the presence of the sporadic-E layer itself. If the effect of the flare is to alter the bulk density of the ionosphere, then this would be on a spatial scale larger than that which is expected to cause ionospheric structures observed by LOFAR. These results indicate that enhanced levels of geomagnetic and solar activity are not the primary drivers of the ionospheric plasma structures observed by LOFAR. The heliogeophysical conditions of $K_p > 4$ or $F_{10.7} > 150$ sfu are relatively rare within the dataset (Figure 2) but, when these conditions do occur, ionospheric structures are more likely to be observed. There were 179 observations when $K_p > 4$, and ionospheric structures occurred in 41 (23 %) of these observations. There were 246

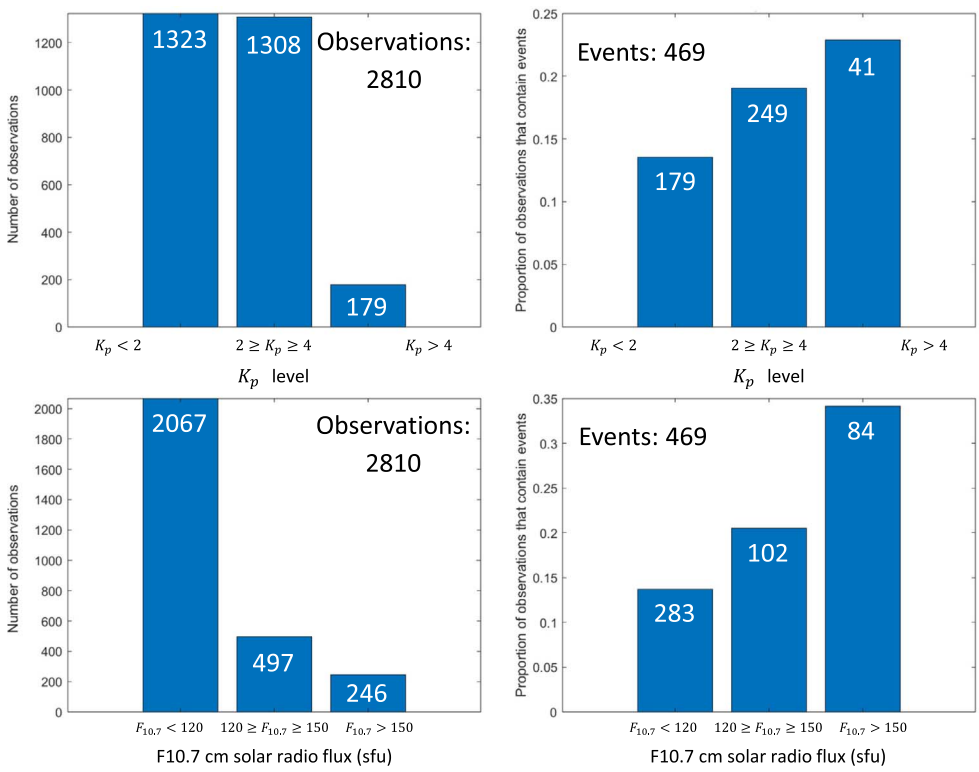

Figure 2. The number of hours of observations in the dataset for three different ranges of the K_p index (top left panel) and the F10.7 cm solar radio flux (lower left panel), together with the proportion of hours in the dataset which contain events in the same ranges of the K_p index (upper right panel) and the F10.7 cm solar radio flux (lower right panel). The total number of observations or events that comprise each bar on the panels is also shown.

observations when $F_{10.7} > 150$ sfu, and ionospheric structures occurred in 84 (34%) of these observations. These exceeded the general occurrence rate of ionospheric structures in the dataset, which was 17% (ionospheric structures occurred in 469 out of 2810 observations). Elevated values of $F_{10.7}$ are used as a proxy for increased photoionisation of the upper atmosphere. A wave that induces a perturbation of $\Delta N\%$ is more likely to produce an observable effect upon a transionospheric radio wave when the background density N is elevated, as proposed by Aarons (1982) and observed by Jenner et al. (2020). Therefore, it may be that it is easier to see the effects of waves originating in the lower atmosphere when $F_{10.7}$ is elevated, and this may be a reason why a greater proportion of the observations in the higher category of $F_{10.7}$ contain events. Collectively, these results indicate that elevated heliogeophysical conditions are a secondary effect.

The proportions of observations in the dataset that contain events are shown as a function of time of day and of month in Figure 3. The conversion from UT to local time (LT) is approximately UT + 1 h. This conversion is not exact due to the apparent motion of the radio source. The elevation and azimuth of Cassiopeia A vary with both the time of day and season, altering the location at which the ray path intersects the ionosphere and the conversion from UT to LT. The frequency of events increased in the evening, peaking at night between 20 UT and 01 UT (approximately 21 LT – 02 LT). The variation as a function of season shows that events are more frequent in summer, with a peak in June and July. Figure 3 also shows lightning strike data as a function of season and hour of the day. These data were taken from ATDNet between 2014 and 2016 to cover the years of the LOFAR observations. The spatial extent considered for the lightning strike data was 51.9° N – 56.5° N and 3.9° E – 9.9° E. This range was set by assuming that the ionospheric structures were at an altitude of 120 km, as this was the altitude of an ionospheric structure observed by LOFAR in Wood et al. (2024). The latitudinal and longitudinal range of the ionospheric intersection of the line-of-sight path between the radio source and the receiving station was then determined. This range was then extended in each direction by 100 km. The number of lightning strikes maximises in summer in the late afternoon (Figure 3, bottom left panel). The number of hours that contain at least one lightning strike (Figure 3, bottom right panel) also peaks in summer in the late afternoon. A similar variation with season and UT was observed for the ionospheric structures observed by LOFAR, although they showed a peak occurrence at a later UT. Such a delay is not unexpected. Azeem et al. (2015) conducted a multi-instrument study to observe an AGW that arose from a convective storm, where the AGW propagated upwards through the atmosphere. The ionospheric signatures were observed in the following hours.

The mean, standard error in the mean, and median number of lightning strikes per hour for observations in the dataset when events occurred, and observations where no events occurred are shown in Table 1. These data are shown for the hour of the LOFAR observations and up to six hours earlier. This satisfactorily covers the time difference between large tropospheric storm cells and thunderstorm-induced gravity waves in the upper mesosphere as observed in airglow images (at 85–

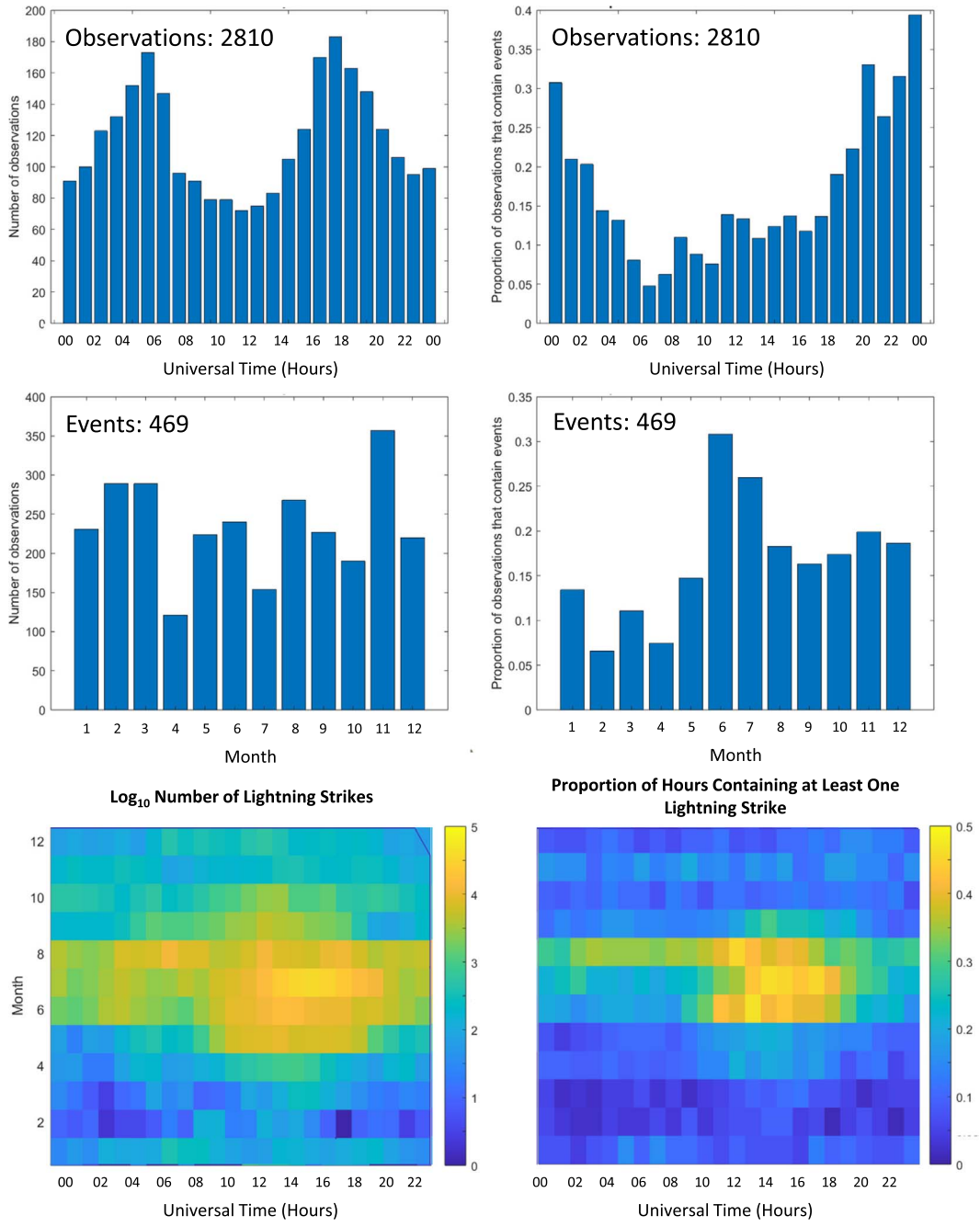

Figure 3. As Figure 2, but for hours of the day (top row) and month of year (middle row). Also shown are the number of lightning strikes per hour (lower left panel) as a function of UT and month for 2014–2016 for a region bounded by latitudes of 51.9° N – 56.5° N and longitudes of 3.9° E – 9.9° E, and the number of hours in this interval that contain at least one lightning strike (lower right panel).

90 km height). Satellite observations and modelling efforts have determined the characteristic velocities of thunderstorm-induced AGWs. Taylor & Hapgood (1988) showed that thunderstorms were a source of short-period AGWs in the atmosphere. Vadas et al. (2012) showed that such AGWs observed in airglow are typically generated between 1 and 5 h previously by strong plumes of thunderstorm cells. At times, AGWs in the upper atmosphere are even observed simultaneously with the tropospheric thunderstorm (see, e.g., Miller et al., 2015). Table 1 shows the mean number of lightning strikes for hours when ionospheric events occurred, maximised two hours before the LOFAR observations with a value of (70 ± 25) lightning strikes per hour, with the uncertainty given by the standard error in the mean. This was greater than the equivalent value for when ionospheric events did not occur, which was (19 ± 5) lightning strikes per hour. If the lightning strike data are assumed to follow a Poisson distribution (Petrov & D'Alessandro, 2002), then the 95% confidence interval is given by Mean Value ± (1.96· Standard Error in the Mean). Under this assumption, the difference between the mean number of lightning strikes per hour when ionospheric events occurred or when they were absent is statistically significant at the 5% level.

Table 1. Lightning strike data from the Arrival Time Differing NETwork (ATDNet) for hours in the dataset when events occurred, and hours where no events occurred. The mean, standard error in the mean, and median values are shown for the hour of the LOFAR observations and up to six hours earlier.

Number of hours before LOFAR observations	Events			Non-events		
	Mean	Standard error	Median	Mean	Standard error	Median
0	40	14	0	19	6	0
1	65	24	0	18	5	0
2	70	25	0	19	5	0
3	54	15	0	18	3	0
4	50	13	0	19	3	0
5	57	19	0	20	4	0
6	52	13	0	25	6	0

The assumption that the ionospheric structures were at an altitude of 120 km is a sensible starting point for this initial statistical study based on the information available to date. This choice should be revisited and will likely need to be revised as additional studies are conducted. However, the basic seasonal and temporal pattern of lightning strikes is robust against the changes caused by variations in the ionospheric structures. This is discussed in detail in Supplementary Material 2.

Lightning strikes can be taken as a proxy for thunderstorm activity. Convective overshooting, where a thunderstorm breaks through the tropopause, can generate a broad spectrum of AGWs. The overshooting tops are the upper part of the storms where strong convective updrafts penetrate the cloud-top equilibrium level and break up to a few kilometres into the lower stratosphere. The resulting ionospheric effects have both been observed (e.g., Azeem et al., 2015) and modelled (e.g., Lu et al., 2024). It is suggested that thunderstorms may launch AGWs, which ultimately cause some of the ionospheric structures observed by LOFAR. In summer, the reversal of the background wind in the mesosphere and stratosphere causes AGWs launched by thunderstorm activity to break or dissipate in the mesopause. It has also been shown that secondary AGWs launched when the primary gravity waves break can ultimately reach ionospheric altitudes (Vadas et al., 2018).

Thunderstorm activity may explain some, but not all, of the ionospheric structures observed. The median value of the number of lightning strikes in every row of Table 1 is zero. This indicates that lightning is a relatively rare phenomenon, but when it does occur, ionospheric structures are likely to follow. However, the lag of two hours between the lightning strikes and the ionospheric structures observed by LOFAR is significantly less than the seven-hour lag between the peak occurrence of lightning strikes (which peaked between 16–17 UT in July) and the peak occurrence of events observed by LOFAR (which peaked between 23–00 UT when all months were combined). While it appears that thunderstorms may launch AGWs that cause some of the ionospheric structures observed by LOFAR, they are not the only source of these structures. The proportions of observations in the dataset that contain events also show an asymmetry between autumn and spring, with a greater proportion of events in autumn. This may be a consequence of the atmospheric conditions, and proxies for the variability of the atmosphere need to be considered.

The relationship between several indices that act as proxies for atmospheric variability and the presence or absence of ionospheric events in the LOFAR dataset is shown in Figure 4. The indices chosen are the North Atlantic Oscillation (NAO) index, the planetary wave activity index, the potential energy density of AGWs, and the Northern Annular Mode (NAM) index. The NAO index is a well-established proxy for the strength and direction of the westerly winds and storm tracks above the Atlantic Ocean (Hurrell et al., 2003). The NAO index was centred on zero, following a quasi-normal distribution. The planetary wave activity index and the gravity wave potential energy density (GWPED) are provided at stations across Europe, and the data used in the present study are from observations at UFS, Germany (47.04° N; 10.98° E) as out of the stations which had data available during the interval of the LOFAR observations, this was the closest to the LOFAR station CS032. The planetary wave activity index and GWPED of AGWs followed a quasi-Gamma distribution with a long tail to higher values. The values of the median and quartiles, which were used to set boundaries between different categories, are based on all of the data available for the NAO index (1st January 1950 – 31st May 2024) and all available data for the planetary wave activity index (July 2009 – June 2024). In the case of the GWPED, all data available for this index between 28th June 2014 and 27th November 2016 were used to find the median and quartile values. In each case, the dataset that was used to find the median and the quartiles is different from the hours for which LOFAR observed, so there will not necessarily be ~25 % of observations in each bin. This is particularly apparent for the GWPED, where Figure 4 shows that the majority of LOFAR observations occurred within the category "lower quartile – median". This could be a consequence of the seasonal variation in the GWPED (not shown) and the uneven distribution of LOFAR observations with season. The month that has, on average, the lowest value of the GWPED is July, which is one of the months with a relatively low number of LOFAR observations (Figure 3). The NAM index is a measure of the strength of the polar vortex and is calculated at a pressure level of 10 hPa. This index was split into three categories, which were NAM index < -3, $-3 \geq$ NAM index ≤ 2 and NAM index >2. These correspond to the weak, stable, and strong polar vortices, respectively (Gerber & Martineau, 2018; Kumar et al., 2025).

The proportion of events in the different categories of the NAO index was broadly similar, indicating that the location and strength of the eastward storm tracks across the Atlantic Ocean do not influence AGWs considered in the present study.

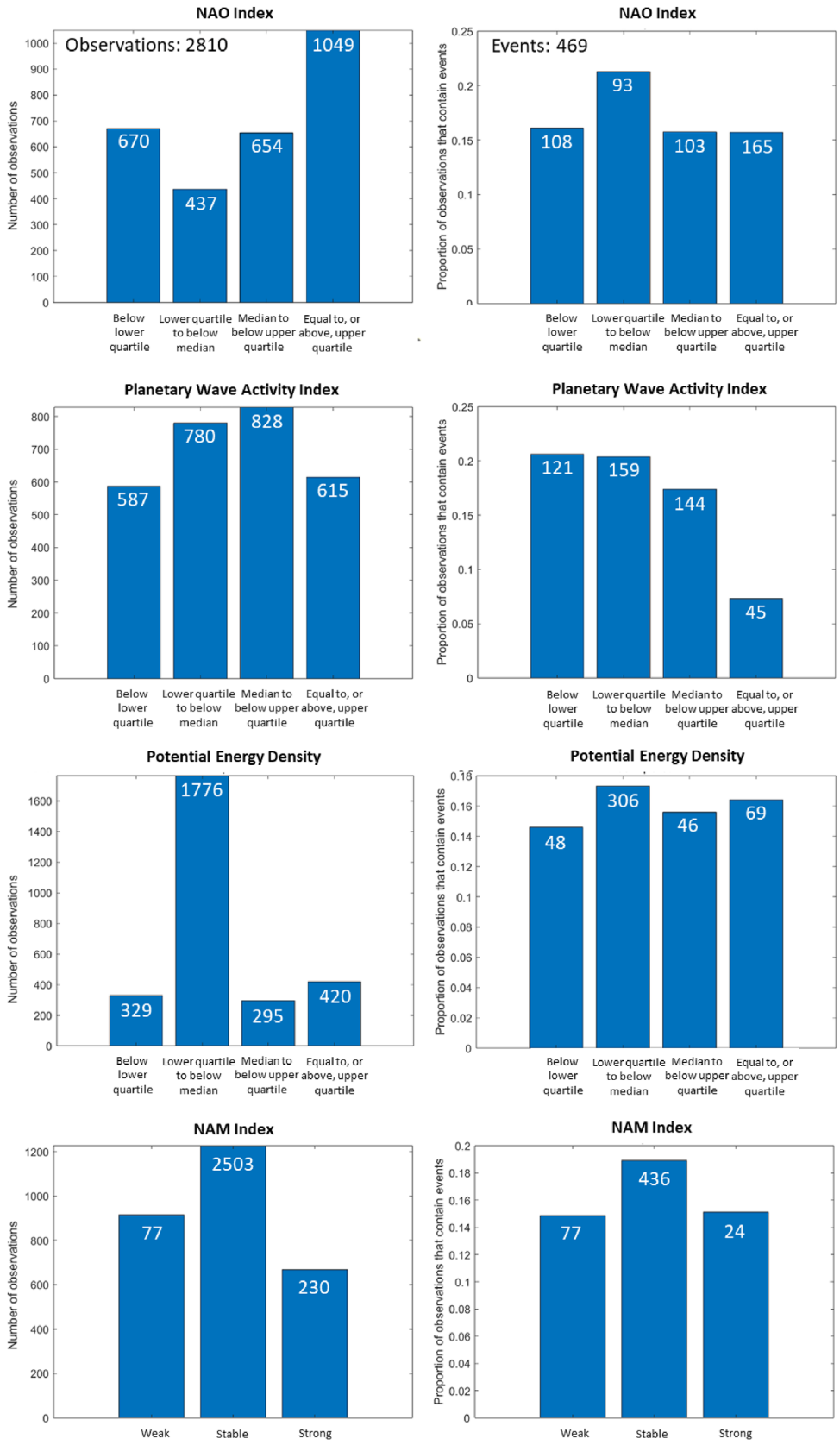

Figure 4. As Figure 2, but for the NAO index (top row), the planetary wave activity index (second row), the potential energy density of AGWs (third row), and the NAM index (lower row). The planetary wave activity index and the potential energy density of the AGWs were observed at the Environmental Research Station (UFS) at Schneefernerhaus, Germany (47.04° N; 10.98° E).

The proportion of observations in which ionospheric events occurred was greater when the planetary wave activity index was lower, suggesting that less disturbed conditions are more favourable for the propagation of the waves that caused the ionospheric disturbances. However, this relationship needs to be treated with caution as more ionospheric events are observed in summer, while the planetary wave activity index exhibits a strong seasonality with smaller values in summer and larger values in winter.

The proportion of observations for the GWPED in which ionospheric events occurred did not vary with the value of the GWPED (Figure 4, third row). At first, this comment appears to be contradictory to many of the other arguments presented in this paper. However, the location at which this potential energy density was calculated (47.04° N; 10.98° E) was ∼700 km from the LOFAR station CS032. This distance is less than the scale size of a planetary wave, but significantly greater than the scale size of an AGW. In addition, UFS observations are performed above the Alps, where the AGW spectrum is expected to be dominated by AGWs of orographic origin. Due to the prevailing wind systems and propagation patterns, these Alpine orographic AGWs are hardly observable from the Netherlands. Therefore, it is not surprising that there is no apparent relationship to the ionospheric structures observed by LOFAR.

The proportion of observations in which ionospheric events occurred varied with the NAM index, with a greater proportion of events occurring when this index was stable. All instances when the polar vortex is strong, as indicated by NAM index > 2, occurred between 7th December and 16th March. A strong polar vortex can alter the mean wind and, hence, the propagation conditions for the AGWs. This may be the reason why fewer ionospheric events are observed in late winter and early spring (January – March) than in autumn and midwinter (September – December). However, as there were relatively few observations in the dataset under conditions when the polar vortex was classed as weak (78 h) or strong (230 h), these comments should be treated with caution. If these ionospheric structures are located at an altitude of 120 km or below, then, based upon the azimuth and elevation of the radio source, all of the LOFAR observations are equatorward of ∼56° N. It would be interesting to conduct additional observations using a radio source at a lower elevation, which would enable observations closer to the polar vortex for all categories of the NAM index.

Another potential source of AGWs is orography. An 18-year global climatology of gravity wave momentum flux showed that orography, specifically the flow over the Scottish mountains, was a significant source of AGWs over the North Sea (Hindley et al., 2020). As the LOFAR observations used in the present study intersect the ionosphere in a region over the North Sea close to the Dutch coast (the northward and westward boundaries of this region being ∼56° N and ∼ 4° E, respectively), it seems unlikely that there is a major orographic source of AGWs in the present study. However, the radio source Cygnus A has been used increasingly regularly in the LOFAR Ionospheric Scintillation experiment since May 2016, in addition to Cassiopeia A. The position of Cygnus A (RA: 299.87°; Dec: 40.73°) results in lower-elevation paths that intersect the ionosphere over the North Sea further north and west of those associated with Cassiopeia A (RA: 350.85°; Dec: 58.82°) in the present study, and so the idea of an orographic source may need to be reconsidered when these observations from Cygnus A are analysed.

The propagation of AGWs is strongly affected by the background conditions. The mesospheric and lower thermospheric winds, planetary waves and tides play roles in the modulation of the wave propagation capable of arriving at ionospheric altitudes. The background wind climatologies have winter and summer conditions and transition seasons (spring and autumn). The springs show more variability and depend on the final breakdown of the polar vortex before the arrival of the summer conditions, while the autumn transition is more abrupt and occurs during the same week at middle latitudes (Jaen et al., 2022). The solar semidiurnal tide and non-migrating tides play a significant role during the spring and autumn transitions and contribute to the evidenced asymmetry between the two seasons. Conte et al. (2018) identified that in spring, the solar semidiurnal non-migrating westward-propagating tide (SW1) is slightly more active than in autumn, influencing the migrating semidiurnal tide (SW2). The propagation of AGWs is strongly affected by planetary waves and tides as they modulate the mean background wind (Baumgarten et al., 2018). The sources of AGWs and the conditions that are needed for them to be able to affect ionospheric altitudes vary with both local time and season. There are insufficient LOFAR observations in the present study to enable the dataset to be broken down by local time and season simultaneously. However, as this dataset continues to expand, this will become possible and will give a clearer insight into the underlying physical processes.

5 Discussion

The daily and seasonal patterns of ionospheric structures shown in Figure 3 show that the proportion of observations in which ionospheric structures were observed increased in the evening, peaking at night between 20 UT and 01 UT (approximately 21 LT – 02 LT). Such structures were more frequent in summer, with a peak in June and July. These patterns are similar to, but not the same as, those reported by Dagg (1957). This earlier study reported that the peak daily occurrence was in the evening at around 21 LT and that the peak seasonal occurrence was between April and June (inclusive). The reasons for this difference may include the differences in the geophysical conditions, the observing frequency, and the location observed. The observations of Dagg (1957) were 4° N and 11° W of those used in the present study. This means that these observations were closer to the polar vortex and also that the orographic effects were likely to be more prominent.

The patterns of occurrence of the ionospheric structures with seasonal and local time patterns showed similarities to the occurrence of lightning strikes. The mean number of lightning strikes two hours before the LOFAR observations, when ionospheric structures were present, was (70 ± 25) per hour, which was significantly larger than the value of (19 ± 5) per hour when ionospheric structures were absent. This suggested that quasi-upward propagating AGWs launched by thunderstorm activity could be one of the sources of the ionospheric structures. It may be that these AGWs break around the mesopause, but as these waves break, they can launch secondary AGWs, and these

waves can reach ionospheric altitudes. AGWs can also be launched by processes including fronts, baroclinic instabilities in the troposphere, and the excitation of waves associated with the polar vortex. The present study does not exclude these sources of AGWs; indeed, the role of some of these sources may be masked by the seasonal bias in the present dataset. As additional LOFAR observations are processed, this dataset will expand, and it is anticipated that any seasonal bias that remains can be removed by stratified sampling. It should also be noted that all of the indices used within the present study are proxies for the underlying physical processes; they are not a perfect representation of the processes themselves. Therefore, case studies may give a deeper insight into the role of the underlying physical processes. Even for thunderstorms, further observational and modelling studies are recommended. A particularly promising location for conducting case studies of AGWs launched by thunderstorms is in northern Germany, where, at certain times of day, the line-of-sight path from LOFAR station DE604 (52.4° N; 13.0° E) passes through the fields of view of the ionosonde, meteor radar, and Medium Frequency (MF) radar located at Juliusruh (54.6° N; 13.4° E). New, high-quality airglow observations are available from Wuppertal (51.3° N; 7.2°E), which would reduce the geographical offset between the mesospheric and ionospheric observation sites used in this study. Co-ordinated, multi-instrument studies may be able to simultaneously observe AGWs and ionospheric structures arising from sources lower down in the terrestrial atmosphere. Modeling studies may be able to suggest the precise mechanism(s) by which such AGWs result in ionospheric structures.

Thunderstorms are associated with deep convection in convectively unstable regions of the lower atmosphere. The precise mechanism(s) that generate these are beyond the scope of the present study. However, it is interesting to note that some authors have proposed a link between lightning and space weather. For example, Owens et al. (2014) showed that lightning and thunder rates in the UK were modulated by the polarity of the Interplanetary Magnetic Field (IMF).

The present study indicates that enhanced levels of geomagnetic and solar activity are not the primary drivers of the ionospheric structures observed by LOFAR. However, it is likely that elevated heliogeophysical conditions are a secondary effect. The heliogeophysical conditions of $K_p > 4$ or $F_{10.7} > 150$ sfu are relatively rare, but when such conditions occur, ionospheric structures are more likely to be observed. When $K_p > 4$ ionospheric structures occurred in 23% of observations, and when $F_{10.7} > 150$ sfu ionospheric structures occurred in 34% of observations. In both cases, this exceeded the general occurrence rate of 17%. Ionospheric structures have been attributed to heliogeophysical conditions previously. Fallows et al. (2020) observed two TIDs simultaneously with LOFAR and suggested that one of these may be associated with a weak substorm. Extreme heliogeophysical events can result in ionospheric structures that are observed by LOFAR. Ghidoni et al. (2025b) used LOFAR to observe the ionospheric effects of the May 2024 geomagnetic superstorm, during which K_p peaked at $K_p = 9$ and several X-class flares occurred. Geomagnetic storms have also been shown to cause disturbances in the background mesospheric and lower thermospheric winds, which change the filtering conditions for propagation of the AGWs (Li et al., 2019; Jaen et al., 2023).

In the present study, ionospheric structures were defined as being present when the 95th percentile of S_4^{180} at 44.3 MHz observed across ~1 h exceeded 0.1. It must be emphasised that this definition was intended to be a starting point for this initial statistical study. As the definition was created based upon observations of SSTIDs and variations within a sporadic-E layer, it may be more sensitive to these physical effects than other phenomena. This definition should be revisited and will likely need to be revised as additional studies are conducted.

The altitude of the ionospheric structures in the present study is poorly constrained. While these altitudes can, occasionally, be determined from the LOFAR observations themselves (e.g., Fallows et al., 2020) or by using complementary instrumentation (e.g., Wood et al., 2024), frequently neither option is practical (e.g., Trigg et al., 2024). The LOFAR ionospheric scintillation experiment uses two astronomical radio sources. The current version, which has run since May 2016 (LOFAR Observing Cycle 6), uses Cassiopeia A (used in the present study; RA: 350.85°; Dec: 58.82°) and Cygnus A (RA: 299.87°; Dec: 40.73°). If this experiment were modified to include other strong, compact radio sources, and if different sources were used for observations made at different LOFAR stations, then experiments could be devised with intersecting ray paths for the lines of sight between the different radio sources and the receivers. Triangulation could then be used to identify a range of altitudes over which the ionospheric structures are located.

Global Circulation Models (GCMs) are widely used by meteorological organisations around the world. For example, the Thermosphere-Ionosphere-Electrodynamics General Circulation (TIE-GCM) model (Dickinson et al., 1981; Richmond et al., 1992; Qian et al., 2014) is the background model for the Advanced Ensemble Networked Environment Assimilation System (AENEAS; Elvidge & Angling, 2019), which is being deployed operationally for the UK Met Office (UKMO). Despite the wide applications of GCMs, there are also limitations. A major outstanding issue is that GCMs do not fully account for the effects of AGWs (e.g., Sun et al., 2023). This dramatically inhibits the ability of these models to accurately represent the global atmospheric circulation. LOFAR enables detailed observations of the ionospheric effects of AGWs at locations spanning central and western Europe. Such observations have the potential to be used to test and validate future developments to GCMs.

6 Conclusions

Results are presented from a statistical study using 2,810 hours of observations of Cassiopeia A (RA: 350.85°; Dec: 58.82°) from a LOFAR station located in the Netherlands (station CS032; 52.9° N; 6.9° E) between 28th June 2014 and 27th November 2016. Ionospheric structures were identified in 469 (~17 %) of these observations. The K_p index was used as a proxy for geomagnetic activity, and the F10.7 cm solar radio flux was used as a proxy for solar activity. It was shown that neither geomagnetic activity nor solar activity was the driver for the majority of these ionospheric structures. Ionospheric structures were more common in summer than in winter, and between 20 UT – 01 UT (~21 LT – 02 LT) than at other times

of day. These patterns in season and local time showed similarities to the occurrence of lightning strikes. The mean number of lightning strikes two hours before the LOFAR observations when ionospheric structures were present was (70 ± 25) per hour, which was substantially larger than the value of (19 ± 5) per hour when ionospheric structures were absent. This suggested that quasi-upward propagating AGWs launched by thunderstorm activity could be one of the sources of the ionospheric structures. Other potential sources of AGWs are not excluded, and further observational and modelling studies are recommended.

Collectively, the observations presented in the present study show that LOFAR can observe ionospheric signatures of vertical coupling processes in the mid-latitude atmosphere. As well as enabling studies of vertical coupling in the terrestrial atmosphere, such observations have the potential to be used to test and validate existing Global Circulation Models (GCMs). They could also be used to develop new models of vertical coupling in the terrestrial atmosphere.

Acknowledgements

The authors gratefully acknowledge Prof. Dan Marsh (University of Leeds) for the useful conversations about the potential impact of this work for General Circulation Models. This paper is based on data obtained with the International LOFAR Telescope (ILT) ionospheric scintillation experiments. LOFAR (van Haarlem et al., 2013) is the Low Frequency Array, designed and constructed by ASTRON. It has observing, data processing, and data storage facilities in several countries that are owned by various parties (each with their own funding sources) and that are collectively operated by the ILT foundation under a joint scientific policy. The ILT resources have benefited from the following recent major funding sources: CNRS-INSU, Observatoire de Paris and Université d'Orléans, France; BMBF, MIWF-NRW, MPG, Germany; Science Foundation Ireland (SFI), Department of Business, Enterprise and Innovation (DBEI), Ireland; IO, The Netherlands; The Science and Technology Facilities Council, UK; Ministry of Science and Higher Education, Poland. The UK Met Office's Arrival Time Difference Network (ATDnet) lightning location data was provided by the UK Met Office. Airglow observations at UFS have been supported by the Bayerisches Staatsministerium für Umwelt und Verbraucherschutz (BayStMUV projects including GUDRUN, grant no. 71b-U8729-2003/125-13; GRIPS3 Back-Up, 2009/40051; BHEA, TLK01U-49580; LUDWIG, TUS01UFS-67093; VoCaS, TKP01KPB-70581; and AlpEn-DAC, TUS01UFS-72184). The mesospheric planetary wave activity and GWPED are indices that have been created as part of the "QUiet Ionospheric Disturbances REsearch based on Ground-based mesospheric and Ionospheric data with Swarm data" (QUID-REGIS) project funded by the European Space Agency (ESA Contract No. 4000143632/24/IEB), which investigates the dynamics of the quiet ionosphere. The editor thanks two anonymous reviewers for their assistance in evaluating this paper.

Funding

This work was supported by the Leverhulme Trust under Research Project Grant RPG-2020-140. Alan Wood, Gareth Dorrian and Ben Boyde gratefully acknowledge funding from this source. Carsten Schmidt, Jaroslav Urbář, Lisa Küchelbacher, Patrick Hannawald, Petra Koucká Knížová and Vladimír Truhlíkwere supported by ESA contract No. 4000143632/24/I-EB (QUID-REGIS). Alan Wood, Gareth Dorrian and Jaroslav Urbář were supported by ESA contract No. 4000143413/23/I-EB (Swarm-VIP-Dynamic). Alan Wood, Rosie Johnson, and Biagio Forte were supported by the United Kingdom Natural Environment Research Council (NERC) grant EISCAT3D: Fine-scale structuring, scintillation, and electrodynamics (FINESSE) (NE/W003147/1, NE/W003074/1, and NE/W002914/1). Sean Elvidge, Neil P. Hindley, and Juliana Jaen were supported by the United Kingdom Natural Environment Research Council (NERC) grant EISCAT3D: DRivers and Impacts of Ionospheric Variability with EISCAT-3D (DRIIVE) (NE/W003368/1 and NE/W003201/1) project. Neil P. Hindley was supported by the United Kingdom Natural Environment Research Council (NERC) grant searching for Upper Atmospheric Waves at the Edge of Space (SURGE) (NE/X017842/1) and TEAMx-FLOW: Flow Dynamics, Scale Interactions and Mountain Waves for TEAMx-UK (NE/Z50399X/1). Juliana Jaen was also supported by the United Kingdom Natural Environment Research Council (NERC) grant Mesospheric sub-Seasonal to Decadal predictability (MesoS2D, NE/V01837X/1). Martin Füllekrug was supported by Natural Environment Research Council (NERC) grants Radio Tomography for Atmospheric Science (NE/L012669/1) and Relativistic Electron Beams Above Thunderclouds (NE/H024921/1), and Royal Society grant NMG/R1/180252. Biagio Forte was supported by Natural Environment Research Council (NERC) grants Space weather disruptions to satellite navigation and telecommunications: ionospheric scintillation (NE/R009082/1) and Space Weather Instrumentation, Measurement, Modelling and Risk: Ionosphere (SWIMMR-I, NE/V002597/1). The CBK PAN group acknowledges the support of the Ministry of Science and Higher Education of Poland through grant no. 30/530252/SPUB/SP/2022, which made this research possible. SRRC/UWM team acknowledges the Ministry of Science and Higher Education of Poland for granting funds for the Polish contribution to the LOFAR ERIC, LOFAR2.0 upgrade (decision number: 2021/WK/2), for the maintenance of the LOFAR PL-612 Baõõldy station (decision number: 28/530020/SPUB/SP/2022) and the Lamkowko Satellite Observatory (decision number: 22/566625/SPUB/SP/2023). Yuriy G. Rapoport acknowledges the National Science Centre, Poland, for granting "Modern radio-diagnostics of the ionosphere using LOFAR and GNSS data" in the OPUS-25 funding initiative under project number UMO-2023/49/B/ST10/03465.

Data availability statement

LOFAR data are available at: https://lta.lofar.eu/, and the light data product used within the present study is available at: https://space-weather.astron.nl/SolarKSP/data/atdb_process/scintillation_preview/. The dates and times used in the present study, together with the 95th percentile of S_4^{180} are shown in the Supplementary Material 1 of the present paper. The geomagnetic index K_p was used as a proxy for geomagnetic activity and was obtained from http://isgi.unistra.fr. The F10.7 cm solar radio flux was obtained from the Laboratory for Atmospheric and Space Physics at https://lasp.colorado.edu. Flares were identified using the Hinode Flare Catalogue (Watanabe et al., 2012). The North Atlantic Oscillation (NAO) index is described in Hurrell et al. (2003). The NAM index is derived under the Scientific Committee on Solar-Terrestrial Physics (SCOSTEP) Visiting Scholar program using the Modern-Era Retrospective analysis for Research and Applications (MERRA-2) data, which is obtained from the Goddard Earth Sciences Data and Information Services Center. https://doi.org/10.5067/A7S6XP56VZWS. Airglow observations at UFS are not publicly available at present. These data will be made publicly available once the QUID-REGIS project concludes.

Supplementary material

Supplementary material 1:

Table S1: The dataset of LOFAR observations from station CS032 used with the present study. This table includes the hour of the observation, the 95th percentile of S_4^{180} for that hour and whether or not

observations were also present at LOFAR stations RS210 and RS310. If the 95th percentile of S_4^{180} exceeded 0.1, then the correlation of relative signal intensity at 44.3 MHz between stations CS032 and RS210, and between CS032 and RS310 is also shown.

Supplementary material 2:

***Table S2*:** Lightning strike data from the Arrival Time Differing NETwork (ATDNet) for hours in the dataset when events occurred, and hours where no events occurred, assuming that the ionospheric structures were located at an altitude of 300 km. The mean, standard error in the mean and median values are shown for the hour of the LOFAR observations, and up to six hours earlier.

***Figure S1*:** The number of lightning strikes per hour (lower left panel) as a function of UT and month for 2014-2016, and the number of the hours in this interval which contain at least one lightning strike (lower right panel) for a region bounded by latitudes of 48.5° N – 60.0° N and longitudes 0.6° W – 14.6° E.

The supplementary material of this article is available at https://www.swsc-journal.org/10.1051/swsc/2026023/olm.

References

Aarons J. 1982. Global Morphology of Ionospheric Scintillations. *Proc IEEE* **70**, **4**, 360–378. https://doi.org/10.1109/PROC.1982. 12314.

Astropy Collaboration, Robitaille TP, Tollerud EJ, Greenfield P, Droettboom M, et al. 2013. Astropy: A community Python package for astronomy. *A&A* **558**: A33. https://doi.org/10.1051/0004-6361/201322068.

Azeem I, Yue J, Hoffmann L, Miller SD, Straka WC, et al. 2015. Multisensor profiling of a concentric gravity wave event propagating from the troposphere to the ionosphere. *Geophys Res Lett* **42**: 7874–7880. https://doi.org/10.1002/2015GL065903.

Baumgarten K, Gerding M, Baumgarten G, Lübken F-J. 2018. Temporal variability of tidal and gravity waves during a record long 10-day continuous lidar sounding. *Atmos Chem Phys* **18**: 371–384. https://doi.org/10.5194/acp-18-371-2018.

Beser K, Mevius M, Grzesiak M, Rothkaehl H. 2022. Detection of periodic disturbances in LOFAR calibration solutions. *Remote Sens* **14** (**7**): 772 1719. https://doi.org/10.3390/rs14071719.

Boyde B, Wood AG, Dorrian GD, de Gasperin F, Mevius M. 2025. Statistics of Travelling Ionospheric Disturbances Observed Using the LOFAR Radio Telescope. *J Space Weather Space Clim* **14**: https://doi.org/10.1051/swsc/2025002.

Boyde B, Wood A, Dorrian G, Sweijen F, de Gasperin F, et al. 2024. Wavelet analysis of differential TEC measurements obtained using LOFAR. *Radio Sci* **59**: e2023RS007871. https://doi.org/10.1029/2023RS007871.

Boyde B, Wood A, Dorrian G, Fallows RA, Themens D, et al. 2022. Lensing from small-scale travelling ionospheric disturbances observed using LOFAR. *J Space Weather Space Clim* **12**: 34. https://doi.org/10.1051/swsc/2022030.

Briggs BH, Parkin IA. 1963. On the variation of radio star and satellite scintillations with zenith angle. *J Atmos Terr Phys* **25**(**6**): 339–366. https://doi.org/10.1016/0021-9169(63)90150-8.

Chum J, Podolská K, Rusz J, Baše J, Tedoradze N. 2021. Statistical investigation of gravity wave characteristics in the ionosphere. *Earth Planets Space* **73**: 60. https://doi.org/10.1186/s40623-021-01379-3.

Clegg AW, Fey AL, Lazio TJW. 1998. The Gaussian plasma lens in astrophysics: refraction. *Astrophys J* **496**: 253–266. https://doi.org/10.1086/305344.

Conte JF, Chau JL, Laskar FI, Stober G, Schmidt H, et al. 2018. Semidiurnal solar tide differences between fall and spring transition times in the Northern Hemisphere. *Ann Geophys* **36**: 999–1008. https://doi.org/10.5194/angeo-36-999-2018.

Dagg M. 1957. Diurnal variations of radio-star scintillations, spread *F*, and geomagnetic activity. *J Atmos Terr Phys* **10**: 204–214. https://doi.org/10.1016/0021-9169(57)90087-9.

Dickinson RE, Ridley EC, Roble RG. 1981. A three-dimensional general circulation model of the thermosphere. *J Geophys Res Space* **86**(**A3**): 1499-1512. https://doi.org/10.1029/JA086iA03p01499.

Dorrian G, Fallows RA, Wood A, Themens DR, Boyde B, et al. 2023. LOFAR observations of substructure within a traveling ionospheric disturbance at mid-latitude. *Space Weather* **21**: e2022SW003198. https://doi.org/10.1029/2022SW003198.

Elvidge S, Angling MJ. 2019. Using the local ensemble Transform Kalman Filter for upper atmospheric modelling. *J Space Weather Space Clim* **9**: 30. https://doi.org/10.1051/swsc/2019018.

Fallows RA, Forte B, Astin I, Allbrook T, Arnold A, et al. 2020. A LOFAR Observation of Ionospheric Scintillation from Simultaneous Medium- and Large-scale Travelling Ionospheric Disturbances. *J Space Weather Space Clim* **10**: 10. https://doi.org/10.1051/swsc/2020010.

Fallows RA, Bisi MM, Forte B, Ulich T, Konovalenko AA, et al. 2016. Separating nightside interplanetary and ionospheric scintillation with LOFAR. *ApJL* **828**: L7. https://doi.org/10.3847/2041-8205/828/1/L7.

Fallows RA, Coles WA, McKay-Bukowski D, Vierinen J, Virtanen II, et al. 2014. Broadband meter-wavelength observations of ionospheric scintillation. *J Geophys Res Space.* **119**: 10544–10560. https://doi.org/10.1002/2014JA020406.

Fritts DC, Vadas SL, Wan K, Werne JA. 2006. Mean and variable forcing of the middle atmosphere by gravity waves. *J Atmos Sol-Terr Phys* **68**: 247–265. https://doi.org/10.1016/j.jastp.2005.04.010.

Fritts DC, Alexander MJ. 2003: Gravity wave dynamics and effects in the middle atmosphere. *Rev Geophys* **41**: 1003. https://doi.org/10.1029/2001RG000106.

Gerber EP, Martineau P. 2018. Quantifying the variability of the annular modes: reanalysis uncertainty vs. sampling uncertainty. *Atmos Chem Phys* **18**: 17099–17117. https://doi.org/10.5194/acp-18-17099-2018.

Ghidoni R, Spogli L, Mevius M, Cesaroni C, Alfonsi L, et al. 2025a. Ionospheric Response to the January 2022 Geomagnetic Storm Using LOFAR and GNSS. *J Space Weather Space Clim* **2025**(**15**): 50. https://doi.org/10.1051/swsc/2025052

Ghidoni R, Spogli L, Dorrian G, Mevius M, Flisek P, et al. 2025b. LOFAR ionospheric capabilities under extreme conditions: The May 2024 Mother's Day Superstorm. *J Space Weather Space Clim* accepted.

Hargreaves JK. 1992. *The solar-terrestrial environment*, Cambridge atmospheric and space science series, Cambridge University Press, ISBN: 9780511628924.

Hindley NP, Wright CJ, Hoffmann L, Moffat-Griffin T, Mitchell NJ. 2020. An 18-year climatology of directional stratospheric gravity wave momentum flux from 3-D satellite observations. *Geophys Res Lett* **47**: e2020GL089557. https://doi.org/10.1029/2020GL089557.

Hines CO. 1960. Internal atmospheric gravity waves at ionospheric heights. *Can J Phys* **38**(**11**): 1441–1481https://doi.org/10.1139/p60-150

Höppner K, Bittner M. 2007. Evidence for solar signals in the mesopause temperature variability? *J Atmos Sol-Terr Phys* **69**: 431–448. https://doi.org/10.1016/j.jastp.2006.10.007.

Holton JR, Hakim GR. 2013. *An Introduction to Dynamic Meteorology* (5th ed.), Academic Press. ISBN: 978-0-12-384866-6. https://doi.org/10.1016/C2009-0-63394-8.

Holton JR 1992. *An Introduction to Dynamic Meteorology*, Academic Press. ISBN: 0-12-354015-1.

Hurrell JW, Kushnir Y, Ottersen G, Visbeck M. 2003. An overview of the north atlantic oscillation. In: J.W. Hurrell, Y. Kushnir, G. Ottersen and M. Visbeck (eds.) *The North Atlantic Oscillation: Climatic Significance and Environmental Impact*. https://doi.org/10.1029/134GM01.

Jaen J, Renkwitz T, Liu H, Jacobi C, Wing R, et al. 2023. Long-term studies of the summer wind in the mesosphere and lower thermosphere at middle and high latitudes over Europe. *Atmos Chem Phys* **23**: 14871–14887. https://doi.org/10.5194/acp-23-14871-2023.

Jaen J, Renkwitz T, Chau JL, He M, Hoffmann P, et al. 2022. Long-term studies of mesosphere and lower-thermosphere summer length definitions based on mean zonal wind features observed for more than one solar cycle at middle and high latitudes in the Northern Hemisphere. *Ann Geophys* **40**: 23–35. https://doi.org/10.5194/angeo-40-23-2022.

Jenner LA, Wood AG, Dorrian GD, Oksavik K, Yeoman TK, et al. 2020. Plasma density gradients at the edge of polar ionospheric holes: the absence of phase scintillation. *Ann Geophys* **38**: 575–590. https://doi.org/10.5194/angeo-38-575-2020.

Kerr F, Shain C, Higgins C. 1949. Moon echoes and penetration of the ionosphere. *Nature* **163**: 310-313. https://doi.org/10.1038/163310a0.

Koval A, Chen Y, Stanislavsky A, Zhang QH. 2017. Traveling ionospheric disturbances as huge natural lenses: solar radio emission focusing effect. *J Geophys Res Space Physics* **122**: 9092–9101. https://doi.org/10.1002/2017JA024080.

Kumar A, Stolle C, Yamazaki Y, Pedatella NM, Kunze M, et al. 2025. Impact of weak and strong stratospheric polar vortices in the northern and southern hemispheres on solar-migrating semidiurnal tides in UA-ICON. *J Geophys Res Atmos* **130**: e2025JD043550. https://doi.org/10.1029/2025JD043550.

Lee ACL. 1989. Ground truth confirmation and theoretical limits of an experimental VLF arrival time difference lightning flash locating system. *QJR Meteorol Soc* **115**: 1147–1166. https://doi.org/10.1002/qj.49711548908.

Li J, Wang W, Lu J, Yue J, Burns AG, et al. 2019. A modeling study of the responses of mesosphere and lower thermosphere winds to geomagnetic storms at middle latitudes. *J Geophys Res Space* **124**: 3666–3680. https://doi.org/10.1029/2019JA026533.

Little C, Lovell A. 1950. Origin of the fluctuations in the intensity of radio waves from galactic sources: Jodrell Bank Observations. *Nature* **165**: 423–424. https://doi.org/10.1038/165423a0.

Lu X, Wu H, Heale C, England S, Zhang S. 2024. Impacts of thunderstorm-generated gravity waves on the ionosphere-thermosphere using TIEGCM-NG/MAGIC simulations and comparisons with GNSS TEC, ICON, and COSMIC-2 observations. *J Geophys Res Space* **129**: e2024JA032854. https://doi.org/10.1029/2024JA032854.

Macotela EL, Clilverd M, Renkwitz T, Chau J, Manninen J, et al. 2021. Spring-fall asymmetry in VLF amplitudes recorded in the North Atlantic region: The fall-effect. *Geophys Res Lett* **48**: e2021GL094581. https://doi.org/10.1029/2021GL094581.

Manson AH, Meek CE, Luo Y, Hocking WK, MacDougall J, et al. 2003. Modulation of gravity waves by planetary waves (2 and 16 d): observations with the North American-Pacific MLT-MFR radar network. *J Atmos Sol-Terr Phys* **65**: 85–104. https://doi.org/10.1016/S1364-6826(02)00282-1

Mayaud PN, 1980. Derivation, meaning, and use of geomagnetic indices. *Geophys Monogr Ser Am Geophys Union.* ISBN:9780875900223. https://doi.org/10.1029/GM022.

McKay-Bukowski D, Vierinen J, Virtanen I, Fallows RA, Postila M, et al. 2014. KAIRA: The Kilpisjärvi atmospheric imaging receiver array – system overview and first results. *IEEE Trans Geosci Remote Sens* **53**(**3**): 1440–1451. http://doi.org/https://doi.org/10.1109/TGRS.2014.2342252

Mevius M, van der Tol S, Pandey VN, Vedantham HK, Brentjens MA, et al. 2016. Probing ionospheric structures using the LOFAR radio telescope. *Radio Sci* **51**: 927– 941. https://doi.org/10.1002/2016RS006028.

Miller SD, Straka WC, Yue J, Smith SM, Alexander MJ, et al. 2015. Upper atmospheric gravity wave details revealed in nightglow satellite imagery. *Proc Natl Acad Sci USA.* **112** (**49**): E6728–E6735. https://doi.org/10.1073/pnas.1508084112.

Owens MJ, Scott CJ, Lockwood M, Barnard L, Harrison RG, et al. 2014. Modulation of UK lightning by heliospheric magnetic field polarity. *Environ Res Lett* **9**: 115009. https://doi.org/10.1088/1748-9326/9/11/115009.

Payne-Scott R, McCready LL. 1948. Ionospheric effects noted during dawn observations on solar noise. *Terr Magn Atmos Electr* **53**(**4**): 429–432. https://doi.org/10.1029/TE053i004p00429.

Petrov NI, D'Alessandro F. 2002. Verification of lightning strike incidence as a Poisson process. *J Atmos Sol-Terr Phys* **64**(**15**): 1645–1650. https://doi.org/10.1016/S1364-6826(02)00135-9.

Price-Whelan AM, Sipöcz BM, Günther HM, Lim PL, Crawford SM, et al. 2018. The Astropy project: Building an open-science project and status of the v2.0 core package. *Astron J* **156**: 123. https://doi.org/10.3847/1538-3881/aabc4f.

Qian L, Burns AG, Emery BA, Foster B, Lu G, et al. 2014. The NCAR TIE-GCM: A community model of the coupled thermosphere/ionosphere system. Modeling the ionosphere–thermosphere system, 73–83. https://doi.org/10.1002/9781118704417.ch7.

Richmond AD, Ridley EC, Roble RG. 1992. A thermosphere/ionosphere general circulation model with coupled electrodynamics. *Geophys Res Lett* **19**(**6**): 601–604. https://doi.org/10.1029/92GL00401.

Schmidt C, Höppner K, Bittner M. 2013. A ground-based spectrometer equipped with an InGaAs array for routine observations of OH (3-1) rotational temperatures in the mesopause region. *J Atmos Sol-Terr Phys* **102**: 125–139. https://doi.org/10.1016/j.jastp.2013.05.001.

Schmidt, C, Küchelbacher L, Wüst S, Bittner M. 2023. OH airglow observations with two identical spectrometers: benefits of increased data homogeneity in the identification of variations induced by the 11-year solar cycle, the QBO, and other factors. *Atmos Meas Tech* **16**(**19**): 4331–4356. https://doi.org/10.5194/amt-16-4331-2023.

Sun YQ, Hassanzadeh P, Alexander MJ, Kruse CG. 2023. Quantifying 3D gravity wave drag in a library of tropical convection-permitting simulations for data-driven parameterizations. *J Adv Model Earth Syst* **15**: e2022MS003585. https://doi.org/10.1029/2022MS003585.

Tapping KF. 2013. The 10.7 cm solar radio flux (F10.7). *Space Weather* **11**: 394–406. https://doi.org/10.1002/swe.20064.

Taylor MJ, Hapgood MA. 1988. Identification of a thunderstorm as a source of short period gravity waves in the upper atmospheric nightglow emissions. *Planet Space Sci* **36**(**10**): 975–985. https://doi.org/10.1016/0032-0633(88)90035-9.

Trigg H, Dorrian GD, Boyde B, Wood AG, Fallows RA, et al. 2024. Observations of high definition symmetric quasi-periodic oscillations in the mid-latitude ionosphere with LOFAR. *J Geophys Res Space* **129**: 2023JA032336. https://doi.org/10.1029/2023JA032336.

van Haarlem MP, Wise MW, Gunst A, Heald G, McKean JP, et al. 2013. LOFAR: The low-frequency array. *A&A* **556**: A2. https://doi.org/10.1051/0004-6361/201220873.

Vadas SL, Zhao J, Chu X, Becker E. 2018. The excitation of secondary gravity waves from local body forces: Theory and

observation. *J Geophys Res Atmos* **123**: 9296–9325. https://doi.org/10.1029/2017JD027970.

Vadas S, Yue J, Nakamura T. 2012. Mesospheric concentric gravity waves generated by multiple convective storms over the North American Great Plain. *J Geophys Res Atmos* **117**: D07113. https://doi.org/10.1029/2011JD017025.

Watanabe K, Masuda S, Segawa T. 2012. Hinode flare catalogue. *Sol Phys* **279**: 317–322. https://doi.org/10.1007/s11207-012-9983-y.

Wood A, Dorrian G, Boyde B, Fallows R, Themens D, et al. 2024. Quasi-stationary substructure within a sporadic E layer observed by the Low-Frequency Array (LOFAR). *J Space Weather Space Clim* **14**: 27. https://doi.org/10.1051/swsc/2024024.

Wüst S, Wendt V, Schmidt C, Lichtenstern S, Bittner M, et al. 2016. Derivation of gravity wave potential energy density from NDMC measurements. *J Atmos Sol-Terr Phys* **138**: 32–46. https://doi.org/10.1016/j.jastp.2015.12.003.

Cite this article as: Wood A, Mevius M, Fallows RA, Jaen J, Dorrian GD, et al. 2026. Driving the mid-latitude ionosphere from below: A statistical study using LOFAR. *J. Space Weather Space Clim*. **16**, 30. https://doi.org/10.1051/swsc/2026023.